analytical chemistry

Article

Cite This: *Anal. Chem.* 2020, 92, 716−723

pubs.acs.org/ac

Ex Situ and *In Situ* Measurement of Water Activity with a MEMS Tensiometer

Winston L. Black II,[†] Michael Santiago,[‡,∥] Siyu Zhu,[†] and Abraham D. Stroock*[,†,§]

[†]Robert Frederick Smith School of Chemical and Biomolecular Engineering, [‡]Sibley School of Mechanical and Aerospace Engineering School, and [§]Kavli Institute for Nanoscale Science and Technology, Cornell University, Ithaca, New York 14853, United States

Supporting Information

ABSTRACT: Water acts as the solvent for natural biotic and abiotic processes and in many technological contexts. The availability of water to participate in chemical and physical processes is captured by thermodynamic variables which track the energetic state of water such as water activity and water potential. Our understanding of the energetic state of water in relevant processes is limited by a lack of sensors capable of providing accurate and reliable *ex situ* and *in situ* measurements of water activity. To address this technology gap, we present applications of a microtensiometer (μTM): a biomimetic microelectromechanical system (MEMS) sensor capable of measuring water activity in liquid, vapor, and semisolid (e.g., hydrogels, cheese) phases. We developed packaging, measurement systems, and methodology to enable us to make water activity measurements previously inaccessible to tensiometry. We present measurements in two contexts: (1) a small benchtop unit for *ex situ* measurements and (2) a probe format for *in situ* measurements. We demonstrate that the μTM can accurately measure water activity in a diversity of complex samples and agrees with chilled mirror hygrometry, an industry standard for water activity measurement.

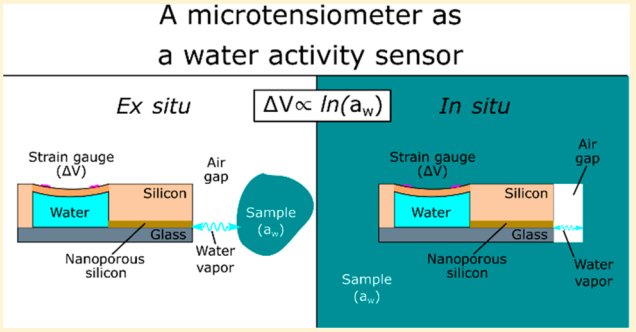

Water activity (or, equivalently, water potential or the chemical potential of water) defines the energetic accessibility of water to participate in chemical and physical processes. In the Supporting Information (SI), section 1, we discuss specific contexts where water activity is relevant.

Despite the broad relevance of water activity, we still lack robust, accurate, and versatile tools for its measurement. Low cost, robust, electrical resistance- or capacitance-based[1] sensors for measuring water activity in vapors (i.e., relative humidity) are widely used for meteorology and monitoring indoor air, but these sensors are insufficiently sensitive for many applications near saturation.[1] For liquid samples, freezing point osmometers can measure water activity, but this technique is inherently limited to making measurements at temperatures near the normal freezing point of water.[2] Membrane osmometers that can measure the osmotic pressure (from which water activity can be calculated) of liquid solutions have been produced commercially[2] and reported in the literature.[3] But, the use of membrane osmometers is uncommon due to factors that complicate their use including solute permeation through membranes. Thermocouple psychrometers have proven useful for both *in situ*[4] and *ex situ*[5] measurements of water activity across a variety of contexts. However, their usefulness is complicated by small, transient, voltage signals, high temperature sensitivity, and the expense of sufficiently precise measurement electronics. Chilled mirror hygrometers provide high accuracy and rapid measurements and have become popular for many applications,[6] but these instruments have been limited to *ex situ* measurements and remain expensive.

We note that these techniques typically require the user to extract samples of the phase of interest for *ex situ* measurement in a dedicated instrument. While there are some techniques which enable *in situ* measurement,[7,8] none of these techniques lend themselves to the creation of probe-type sensors which could be inserted or dipped into a phase of interest.

In this paper, we present a microelectromechanical system (MEMS) tensiometer called a microtensiometer (hereafter, abbreviated as μTM) as a versatile probe to perform *ex situ* and *in situ* measurements of the water activity of complex aqueous samples. We demonstrate the use of this device in two contexts (Figure 2): (1) For *ex situ* measurements on small volumes of samples, we develop a custom measurement system that promotes thermodynamic (i.e., thermal and mass) equilibrium between μTM and the sample of interest. (2) For *in situ* measurements, we developed a probe that allows for complete submersion of the μTM in a sample of interest. The version of the μTM we present is a second generation μTM (the first generation was presented previously[9]). This updated design

Received: June 10, 2019
Accepted: November 25, 2019
Published: November 25, 2019

DOI: 10.1021/acs.analchem.9b02647
Anal. Chem. 2020, 92, 716−723

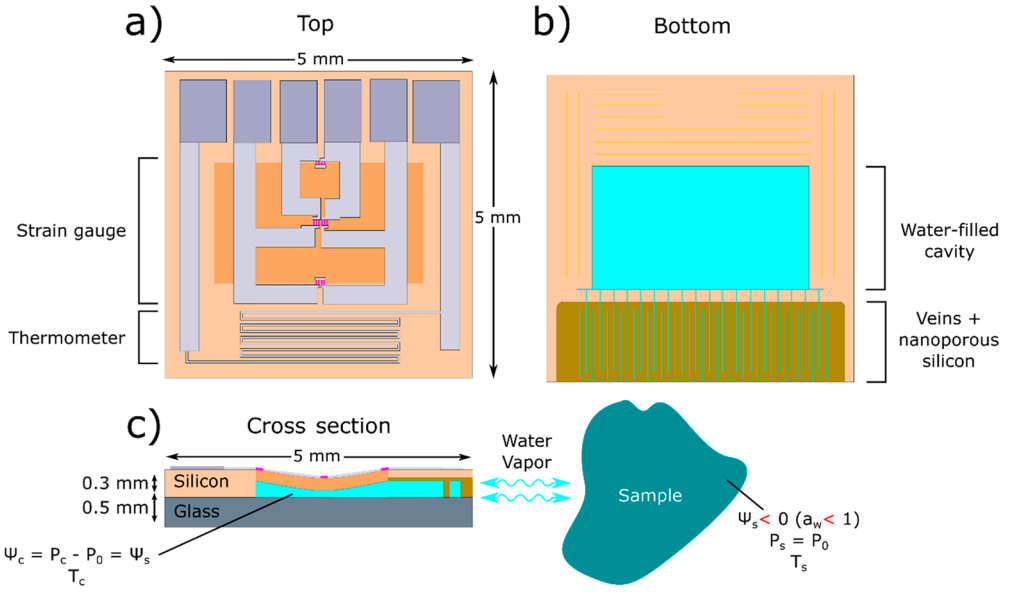

Figure 1. Diagrams of a microtensiometer. (a) Top view. Platinum wiring (light gray), atop silicon oxide (beige), connects a stain gauge to the inner four platinum pads (dark gray) and a thermometer to the outer two pads along the top edge. The strain gauge is composed of four polysilicon piezoresistors (magenta) in a Wheatstone bridge configuration on top of a deformable silicon diaphragm (dark beige). The thermometer is the serpentine thin film of platinum near the lower edge. (b) Bottom view. Looking through a layer of glass, liquid water is visible. Water (light blue) fills a cavity, veins (microscopic etched channels), and the nanoporous silicon (yellow-brown) as it would when the sensor is in use. (c) Cross section in equilibrium with an unsaturated ($\Psi_s < 0$; $a_w < 1$) sample. A cross section of the microtensiometer shows the platinum wiring and the silicon diaphragm (also visible in panel a) as well as the water-filled cavity and veins, porous silicon membrane, and glass layer (also visible in panel b; note that layers are not to scale). After a net transfer of water out of the tensiometer, the pressure in the cavity of the tensiometer is reduced relative to the ambient pressure until equilibrium is reached (i.e., $\Psi_c = \Psi_s$). This reduction in pressure in the cavity causes a downward deflection in the diaphragm.

features veins (Figure 1b) that mimic the xylem of trees to enable faster movement of water through the rigid, porous membrane of the sensor and, therefore, faster response times. Due to the greater operational range of the μTM relative to conventional tensiometers, the work we present here represents an extension of tensiometry into new contexts where the measurement of water activity is important such as food science and process monitoring.

BACKGROUND AND THEORY

Water Activity and Water Potential. Water activity, a_w [-], has one-to-one relationships with two other thermodynamic variables which quantify the energetic state of water: the chemical potential of water, μ_w [J mol^{-1}], and water potential, Ψ [1 bar = 0.1 MPa ~ 1 atm]. These variables are indicative of the partial molar free energy of water and thus capture its ability to move between phases and materials and participate in chemical reactions. In this work, we quantify the free energy of water using water activity and water potential.

We define water activity as follows:

$$a_w = \frac{P_{vap}}{P_{sat}(T)} = \frac{\%RH}{100} \quad (1)$$

where P_{vap} [Pa] is the vapor pressure of a vapor in equilibrium with the water-containing phase of interest, $P_{sat}(T)$ [Pa] is the saturation vapor pressure of water at the sample temperature, T, and %RH [-] is the percent relative humidity. For unsaturated conditions, water activity is between 0 and 1. In fields like food science, water activity is the most commonly used measure of the energetic state of water in a material.

However, since the μTM is a pressure sensor (as we discuss in the next section), we introduce a term from plant and environmental sciences which captures information about the energetic state of water as a pressure:[10] water potential, Ψ [Pa]. Mathematically, water potential is related to water activity as follows:

$$\Psi = \frac{RT}{\nu_w}\ln(a_w) \quad (2)$$

where R = 8.314 J mol^{-1} and is the gas law constant; T [K] is the absolute temperature; and ν_w [m^3 mol^{-1}] is the molar volume of liquid water.

From eq 2, water activity can be calculated from a water potential measurement given the temperature at which the measurement was made. For unsaturated conditions, water potential is less than zero. As we discuss in detail later, the water potential of a pure liquid can also be expressed as the difference between the liquid and ambient pressure:

$$\Psi = P_l - P_0 \quad (3)$$

where P_l [Pa] is the hydrostatic pressure in the liquid, and P_0 is the reference pressure, often chosen to be the ambient pressure (for full derivation, see Pagay et al.).[9] The water potential of a substance includes the following contributions: osmotic, capillary, and hydrostatic pressures.

We discuss relationships between water activity and water potential and other thermodynamics state variables such as the chemical potential of water and osmotic pressure in the SI, section 2.

We note that, as state variables, the chemical potential of water, water activity, and water potential, rather than the water

DOI: 10.1021/acs.analchem.9b02647
Anal. Chem. 2020, 92, 716−723

content or volume fraction, θ [m^3 m^{-3}], are often the most useful measures of the thermodynamic status of water.

Principles of Tensiometry. Though the operation of the μTM has been explained previously,[9] for clarity, we review the principles of operation of the μTM here.

The principles of tensiometry are illustrated in Figure 1c. A volume of pure, bulk water occupies a cavity within a tensiometer. The top of the cavity is a deformable diaphragm (a thin plate of nonporous material; dark beige in Figure 1c) equipped with a strain gauge (magenta lines in Figure 1). The diaphragm and strain gauge deform in response to changes in the pressure within the cavity relative to ambient pressure. Water (light blue in Figure 1) can enter or exit this cavity through a rigid, nanoporous membrane. The water potential (activity) of the sample to which the tensiometer is exposed determines whether water will enter or exit the tensiometer. We note that the sample (dark blue in Figure 1c) could be a water-containing liquid, solid, or semisolid (e.g., hydrogel, cheese), and the following discussion assumes that the sensor and the sample are in thermal equilibrium (i.e., $T_c = T_s$ in Figure 1c).

We note that deviation from isothermal conditions (i.e., $T_c \neq T_s$) can lead to a large error in measurements. The magnitude of this error is about ~8 MPa per degree of temperature difference between the sensor and the sample. We refer to this strong sensitivity to nonisothermal conditions as the psychrometric effect. This effect motivates the design of our experimental systems which promote thermal equilibrium.

When a tensiometer is exposed to a subsaturated sample ($\Psi_s < 0$; $a_w < 1$; Figure 1c), water will exit the cavity, move through the nanoporous membrane, and evaporate at the membrane surface until the pressure in the cavity reaches a reduced pressure: $P_c = P_0 + \Psi_s$. Thus, at equilibrium, the magnitude of the difference between the pressure in the cavity and the ambient pressure equals the water potential of the sample: $P_c - P_0 = \Psi_s$ (eq 3).

This pressure difference causes the diaphragm and strain gauge to deform, and the strain gauge transduces this deformation into a voltage (V_{out}). For the μTM under typical conditions, the deformation of the diaphragm is sufficiently small such that the relationship between stress and strain for the diaphragm is linear. As a result, the difference in the deformed voltage output (V_{out}) and the voltage offset (V_{out}^0) of the strain gauge varies linearly with the pressure difference across the diaphragm and, by extension, the sample water potential, Ψ_s

$$V_{out} - V_{out}^{\ 0} \propto (P_c - P_0) = \Psi_s \tag{4}$$

We perform a calibration to determine the constants in this linear relationship for each device (SI, section 6.2).

To keep liquid water within the tensiometer, the pressure difference between the water in the sensor and the external environment (eq 3) must be balanced by the capillary pressure at the surface of each pore in the porous membrane (Figure 1c). This pressure should follow Young−Laplace law

$$\Psi_s = P_c - P_0 = -\frac{2\sigma\cos(\theta)}{r_p} \tag{5}$$

where σ is the surface tension of water [0.072 N m^{-1}]; θ [rad] is the contact angle of the liquid with the pore wall; and r_p [m] is the radius of a pore at the membrane surface. For stable operation of a tensiometer, the magnitude of the water potential of the sample ($\Psi_s = P_c - P_0$) must not exceed the maximum capillary pressure achievable in the pores of the membrane. This maximum stress is set by the maximum pore radius, $r_{p,max}$, and the receding contact angle of water with the pore wall, θ_r. From eq 5, we have

$$\Psi_{s,min} = (P_c - P_0)_{min} > -\frac{2\sigma\cos(\theta_r)}{r_{p,max}} \tag{6}$$

When $\Psi_s < \Psi_{s,min}$, we expect gas to invade the membrane and eventually the internal cavity such that the liquid tension cannot be maintained. The tensiometer would stop functioning after such an event. Thus, eq 6 illustrates the importance of using a nanoporous membrane in the design of the μTM. Since the minimum measurable water potential ($\Psi_{s,min}$) has an inverse dependence on the radius of the largest pore ($r_{p,max}$), the smaller the largest pore is, the lower the minimum water potential that can be measured is (as seen in eqs 5 and 6). The typical pore size of porous silicon used in the μTM is a few nanometers. If we take $r_{p,max}$ = 10 nm and θ_r = 0, we estimate $\Psi_{s,min}$ = −14.4 MPa. We note that heterogeneous (i.e., surface-activated) nucleation of vapor bubbles within the cavity can also release the tension within the liquid water in a tensiometer. Since we typically observe $\Psi_{s,min}$ ~ O (−10 MPa) and based on videos (see the supplementary movie included with Pagay et al.[9]) of device failure at lower values of $\Psi_{s,max}$ than we predict from eq 6, we believe that cavitation (boiling) by heterogeneous nucleation is the dominant mechanism of failure in the μTM.

METHODS AND MATERIALS

Fabrication. We fabricated μTMs using cleanroom processes in the Cornell NanoScale Science and Technology Facility (CNF) using a 23-step process we developed. We present the full fabrication process in the SI, section 3. Details on this fabrication process are also available elsewhere.[9,11,12]

For our purposes here, we briefly summarize the form and function of the various components of the μTM.

The μTM is the combination of two common sensing circuits: a strain gauge and a thermometer. The thermometer is a serpentine thin film platinum resistance thermometer (PRT; light gray at the bottom of Figure 1a) whose resistance varies as a function of temperature (see eq S6 in the SI). The strain gauge is made of four polycrystalline silicon resistors (magenta in Figure 1a and c) whose resistances vary with strain (i.e., piezoresistors) in a Wheatstone bridge located on a diaphragm. We interface with these sensing circuits via rectangular platinum pads (darker gray rectangles at the top of Figure 1a) and wiring (light gray in Figure 1a). We build these sensing circuits on a layer of silicon oxide (not pictured; to electrically isolate them) atop silicon using photolithography.

Beneath the strain gauge, we etch a 3-μm deep cavity to form a diaphragm (dark beige in Figure 1a and c) and a reservoir of water (light blue in Figure 1b and c). This etch also forms the veins (shown filled with water (light blue) in Figure 1b and c) in an area of porosified silicon (yellow-brown in Figure 1b and c). We note that the veins do not connect directly to each other or to the exterior. Rather, the veins define a segmented path from the cavity to thin sections of nanoporous silicon through which water must pass to exit the μTM. This design was inspired by the segmented structure of xylem vessels and inhibits the penetration of vapor into the cavity or from passing from one vein segment to the next. A

DOI: 10.1021/acs.analchem.9b02647
Anal. Chem. 2020, 92, 716−723

glass wafer anodically bonded to the silicon forms the bottom of the cavity and veins (not visible in Figure 1b; dark gray in Figure 1c).

The result of the fabrication process is a wafer of approximately 150 μTMs with various diaphragm sizes: 1 mm × 2 mm, 1.5 mm × 3 mm, 2 mm × 3 mm, and 3.5 mm × 4 mm. All devices used in this work had a 1 mm × 2 mm diaphragm. We designed the photolithography mask such that some μTMs on each wafer did not have veins (Figure 1b). These devices allowed us to evaluate the impact of the veins on the response time of the μTM.

Packaging. We packaged each μTM individually before use to protect the electronic elements from exposure to high water activity (potential) phases to isolate the diaphragm from mechanical perturbations and promote thermal equilibrium between the μTM and its surroundings. Details on this packaging are available in the SI, section 4.

Systems for Measuring Water Activity. *Ex Situ.* The measurement system we developed for *ex situ* water activity measurements is shown in Figure 2a. Here, "*ex situ*" refers to a measurement performed on a small sample and placed within a measurement system. We use the μTM to measure the water activity of a sample by suspending the sensor over the sample with an air gap (~4 mm thick) between the two. The air gap between the sample and the sensor keeps the water within the sensor pure as long as the sample does not contain volatile chemical compounds. Maintaining a macroscopic vapor gap between the μTM and sample creates challenges in minimizing the temperature difference between the two. To address the challenge of minimizing the temperature difference between sensor and sample, we constructed the measurement chamber out of copper—a material with a high thermal conductivity (Figure 2a). We used a PRT (pictured in Figure 2a) along with a Peltier module and a CPU cooling fan mounted on a stand located under the base to control the temperature of the measurement chamber (not shown in Figure 2a). We used a CR6 datalogger (Campbell Scientific, Logan, UT) to collect data from and power the μTM as well as to control the temperature via a proportional-integral (PI) control scheme. For more detail on this measurement system, refer to the SI, section 5. This measurement system could perform measurements at a user-defined temperature set point. However, for this work, we performed all *ex situ* measurements in this measurement system at 25 °C.

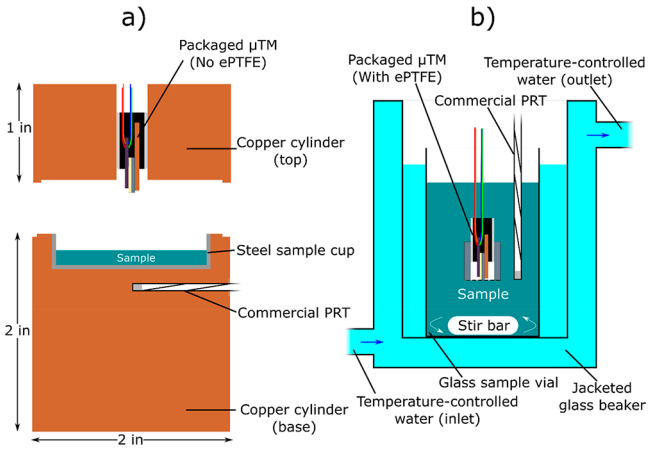

Figure 2. Measurement systems for *ex situ* and *in situ* water activity measurements with a microtensiometer. (a) Diagram of *ex situ* measurement system. A packaged microtensiometer fits into a close-fitting hole in a 2.54 cm tall, 5.08 cm diameter (1 in. tall, 2 in. diameter) copper cylinder. The sample sits in a steel sample cup which fits into a second coper cylinder that is 5.08 cm tall and 5.08 cm in diameter (2 in. tall and 2 in. diameter). A small hole drilled into the side of this cylinder houses a commercial platinum resistance thermometer (PRT). The shorter cylinder containing the microtensiometer is notched to be seated on top of the taller cylinder containing the sample. (b) Diagram of *in situ* measurement system. Temperature-controlled water is pumped through a jacketed glass beaker. A glass sample vial sits within water in the jacketed glass beaker. The glass sample vial contains a sample stirred by a stir bar. A packaged microtensiometer and commercial PRT are suspended within the sample.

In Situ. Here, "*in situ*" refers to measurements performed with the sensor submerged or embedded in the sample of interest. To enable *in situ* measurements of water activity with the μTM, we developed a cap to supplement the basic μTM package. We made these caps from glass tubing and a hydrophobic separator (expanded polytetrafluoroethylene; we refer to this as ePTFE) that defines a microscopic air gap in its pore space (Figure 2b). These caps allowed the sensor to be directly submerged in the sample of interest without contaminating the water within the μTM; the ePTFE separator resisted the permeation of aqueous solutions, only allowing vapors to pass through. Details on the construction of these caps is given in the SI, section 4.

We performed *in situ* measurements by (1) moving the capped μTM and a commercial PRT (Model: HSRTD, OMEGA Engineering, Inc., Norwalk, CT) into a 50 mL vial of stirred sample in a water-filled 200 mL jacketed glass beaker (Ace Glass Inc., Vineland, NJ) whose temperature was regulated by a circulating water bath (Model: NESLAB RTE-17, Thermo Fisher Scientific, Waltham, MA) and (2) waiting until the voltage output of the strain gauge stabilized ($t > 5\tau$; see Figure 5 and the Transients section of Results and Discussion).

In calibration experiments (Figure 3 and Figure 4b), we used a measurement with a jacketed glass beaker (Figure 2b) to keep the μTM and sample of interest at a uniform temperature. For *in situ* in liquid samples (e.g., cell culture medium), we submerged the capped sensor in the liquid of interest. For *in situ* measurements of nonliquid samples (Figure 5), we embedded the sensor (uncapped) directly into the sample.

Again, we used a CR6 datalogger (Campbell Scientific, Logan, UT) to collect data from and power the μTM and commercial PRT.

Uncertainty Analysis. We characterize the uncertainty in the measurements we performed using propagation of uncertainties[13,14] and prediction intervals.[15] Full details on these methods are given in the SI, section 8.

DOI: 10.1021/acs.analchem.9b02647
Anal. Chem. 2020, 92, 716−723

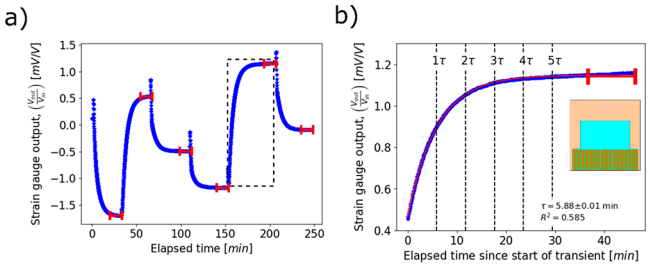

Figure 3. Representative microtensiometer transients and fit to a transient. (a) Strain gauge voltage output (i.e., V_{out}/V_{in}) is plotted as a function of time, as an *in situ* packaged microtensiometer (Figure 2b) is moved to different calibration solutions. Each plateau represents the equilibrium voltage output associated with the sample solution water activity (potential). Samples were aqueous urea solutions (molalities, m [mol urea (kg water)$^{-1}$] of the solutions in order of use: 0 (i.e., deionized water), 3.5, 1.8, 0.8, 4.5, 2.5). The intervals (red) indicate the data points averaged to produce a calibration curve (Figure 4). The dashed black box indicates the transient fit to a single exponential in (b). (b) We fit raw data (blue) from a veined tensiometer (inset) with a single exponential (red; see eq 7) using a least-squares algorithm. The parameter τ [min] is the time constant for equilibration reported on the plot. The dashed black lines indicate multiples of τ along the progression of the transient.

Calibration. We calibrated both the strain gauge and PRT on each μTM. Description of these calibration equations and processes can be found in the SI, section 6.

RESULTS AND DISCUSSION

Transients. Here, we define transients as the response of the μTM as the sensor moves toward equilibrium with the sample. Transients are a practical consideration because the length of the transient determines the time required to perform a measurement. For the μTM, a potential drawback of the nanoporous silicon membrane (which extends its range relative to conventional tensiometers as discussed in the Principles of Tensiometry section) is that the small pore size restricts flow and causes long transients. To address this challenge, we included veins in the design of the μTM. In this section, we discuss the transients of the μTM with veins.

Figure 3 shows a representative set of calibration transients and a fit to a transient for an *in situ* calibration of a μTM with the vein structures as shown in Figure 1b. In Figure 3a, each transient (like the one shown in Figure 3b) represents the relaxation of the μTM toward equilibrium with a solution of known water activity (potential). The increase in the voltage output prior to each transient is the result of the sensor's exposure to ambient air whose water activity (potential) was much lower (more negative) than any of the calibration solutions. The intervals (shown in red) indicate the values we averaged to create a calibration curve (Figure 4). The red curve in Figure 3b is a fitting of the following equation to the data:

$$\frac{V_{out}}{V_{in}}(t) = \Delta e^{-(t/\tau)} + C \tag{7}$$

where Δ, τ, and C are fitting parameters. Graphically, Δ [mV V^{-1}] represents the total change accomplished from the beginning to the end of the transient; τ [min] is the time constant for equilibration; and C [mV V^{-1}] is the final value of the transient. We used fits like the one shown in Figure 3b to determine when the transients were complete. We considered transients to be complete when $t > 5\tau$. Mathematically, when this condition is met, the value of the voltage output (i.e., $\frac{V_{out}}{V_{in}}$) is within 1% of its predicted final value (i.e., C). After $t > 5\tau$, we allowed the transient to progress at least 10 additional minutes. We then averaged the data collected over those 10 min.

On average, *in situ* calibrations had a characteristic time constant, τ, of 3.0 ± 1.3 min (n = 54), and *ex situ* calibrations had a time constant of 3.9 ± 1.8 min (n = 54). The uncertainties we report here are ±1 standard deviation. In the SI, section 9 and Figure S4, we compare the transients for μTMs with and without veins and show that the inclusion of veins reduces the response time over 10-fold relative to a design with no veins. The strategy of adding microstructures to a low permeability membrane, with disconnected segments of

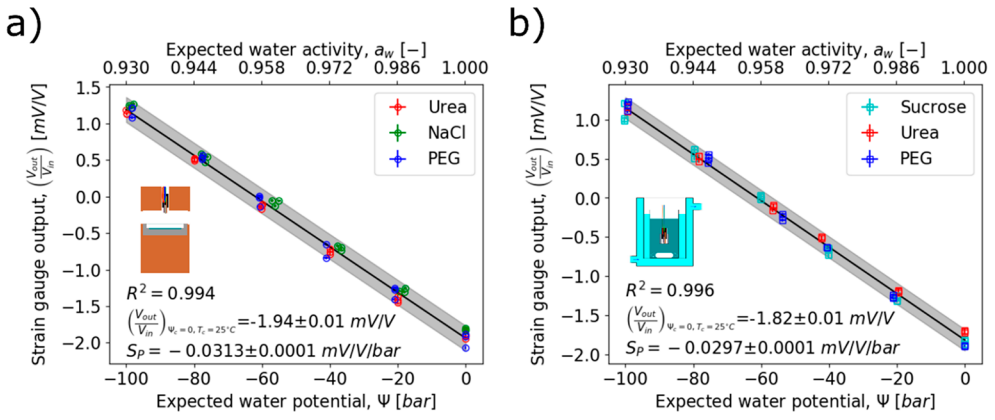

Figure 4. *Ex situ* and *in situ* calibrations of the microtensiometer with various solutes. (a, b) Equilibrium strain gauge voltage output readings (averaged plateau values extracted from calibration time traces, Figure 3) from *ex situ* (a) and *in situ* (b) measurements plotted against the corresponding solution water potentials. Water potentials are reported in units of bars (1 bar = 0.1 MPa ≈ 1 atm) and were either measured with a chilled mirror hydrometer (model WP4C, Meter Group, Pullman, WA) or estimated from literature data (SI, section 6.2). The error bars on both the x- and y-axis were calculated by propagation of errors. The line plotted (black) is a best-fit to all data points on the plot. The slope of this line represents the pressure sensitivity, S_P [mV V^{-1} bar^{-1}]. The gray shaded region indicates the 95% prediction interval denoting the expected range of water potentials or activities predicted from this linear fitting. The confidence internals indicating the uncertainty on the best-fit line are too narrow to be visible on this scale. Inset: diagrams representing the method of measurements used in the plot similar to Figure 2a and b.

DOI: 10.1021/acs.analchem.9b02647
Anal. Chem. 2020, 92, 716−723

microchannels as in plant xylem, could be useful in other membrane applications such as pervaporation.

The time constant we found for the μTM with veins is comparable to the 3−4 min time constant of the chilled mirror hygrometer we used as a reference[16] but slower than the time constants reported for psychrometers[17,18] and electrical resistance- or capacitance-based sensors,[1] which are on the order of seconds to minutes. We assume that the reported "response times" are equivalent to the time constant, τ, and not the time to reach equilibrium (i.e., $\sim 5\tau$). We note that a time constant on the order of minutes is appropriate for most environmental contexts.

Calibrations and Benchmarking. As we have discussed (eq 4), we expect the voltage output of the strain gauge of the μTM to vary linearly with the water potential of the sample. To confirm this linear relationship, determine its constants, and check the reproducibility of the μTM, we followed our strain gauge calibration procedure (SI, section 6.2) for three different solutes for each measurement type (i.e., *ex situ* and *in situ* measurements). For *ex situ* measurements (Figure 4a), we used urea (red data points), sodium chloride (NaCl; green data points), and polyethylene glycol (PEG; blue data points). For *in situ* measurements (Figure 4b), we used urea (red data points), sucrose (cyan data points), and PEG (blue data points). We analyzed data sets like those shown in Figure 3a for solutions of the different solutes to produce Figure 4. For each solute, we collected three data sets using the same solutions on three sequential days to evaluate the variability between measurements. Data points showed no discernible trend with time of collection. We calculated the uncertainty values represented by the plotted error bars on the *x*- and *y*-axis in Figure 4 by propagation of errors. We fit the best-fit line (black solid line) fit to all the data points collected for a given measurement type (*ex situ* for Figure 4a; *in situ* for Figure 4b). From the prediction intervals (gray shaded regions shown in Figure 4a and b), we estimate an uncertainty of $\sim \pm 5.5$ bar for water potentials calculated from the *ex situ* calibration and $\sim \pm 4.6$ bar for water potentials calculated from the *in situ* calibration. These uncertainties have been rounded to the nearest 0.1 bar.

Expected water activity (potential) values (*x*-axis in Figure 4) came from either literature estimates or direct measurements with the WP4C. Clusters of points where there is no variation in expected water activity (e.g., blue PEG data points at $a_w \sim 0.944$ ($\Psi \sim -80$ bar) in Figure 4b) indicate that we estimated expected water activity from literature values for these solutions. We used literature values for a time while the WP4C was unavailable due to required maintenance.

The strain gauge voltage offsets (i.e., $\left(\frac{V_{out}}{V_{in}}\right)$ when $a_w = 1$ ($\Psi = 0$) or $\left(\frac{V_{out}}{V_{in}}\right)_{\Psi=0,T=25\ ^\circ C}$ in eq S7 in the SI) we measured varied between data sets (e.g., urea *in situ*, NaCl *ex situ*). We note that, although we collected the data in Figure 4 with the same sensor over the course of six months, all the variations in the offset lie within the prediction intervals plotted in Figure 4a. However, we observe offset drift in these data. For example, the NaCl *ex situ* data set (green points in Figure 4a) is shifted by some constant offset from the other points on the plot. This shift suggests that offset drift is a significant contributor to the total uncertainty.

We note that there appears to be a difference in slopes between the *ex situ* and *in situ* data (i.e., Figure 4a and b). However, we believe this discrepancy is due to experimental uncertainties (see SI, section 10 for additional discussion).

Those data points in Figure 4 that do not fall on the best-fit line lie within or very near the 95% prediction interval (gray shaded regions) we calculated based on these data. The quantitatively good agreement between the data we collected and the linear model suggests that our approach enables accurate measurements of water activity. Our results do not definitely support or exclude some impact of the psychrometric effect (see SI, section 11 for additional discussion).

Water Activity Measurements. Having calibrated the μTM and demonstrated its reproducibility in aqueous solutions, we turn to using the μTM to perform *ex situ* and *in situ* measurements of water activity (potential) on complex aqueous samples. Figure 5 shows the results from water activity

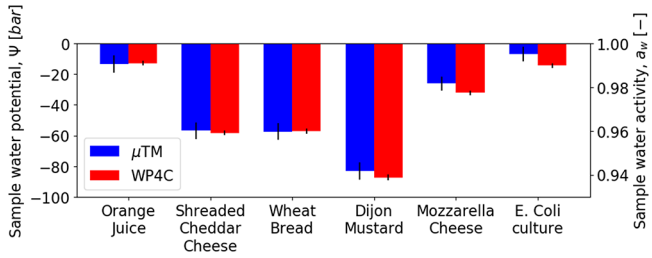

Figure 5. Application of the microtensiometer to measure water activity. Measured water potential (left axis) and activity (right axis) with the microtensiometer (blue) and a chilled mirror hygrometer (model: WP4C; red). The error bars shown on the microtensiometer data are from the 95% prediction interval based on calibration data (Figure 4). The error bars on the WP4C data come from the specifications provided by the manufacture. Measured water potentials were used to calculate water activities using eq 2. We performed *ex situ* measurements on orange juice, cheddar cheese, bread, and mustard at 25 °C. We measured the water potential of mozzarella cheese *in situ* on the benchtop immediately after removing the cheese from refrigeration. We measured the water activity of an active *E. coli* culture *in situ* in a shaking incubator at 37 °C.

(potential) measurements we made on foods and an active cell culture. These samples represent a diversity of chemical compositions and phases. We performed the *ex situ* measurements in the *ex situ* measurement system (Figure 2a), but we did not use the *in situ* measurement system (water-jacketed beaker in Figure 2b) to make the *in situ* measurements. Instead, we performed the mozzarella cheese measurement on a benchtop in a block of mozzarella, newly unwrapped and removed from refrigeration, and we measured the *E. coli* culture in a shaking incubator. We measured the water activity of all samples at 25 °C except for the *E. coli* culture which we measured at 37 °C, the standard cell culture incubator temperature.

The error bars plotted for the μTM are calculated from the prediction intervals presented in Figure 4, and the error bars for the WP4C data come from the manufacture specifications (see SI, section 8 for details). Generally, there is good agreement between measurements made with the μTM and the WP4C. Visually, this agreement is seen in the overlap of the error bars plotted in Figure 5.

We note that we observed a significant difference in measurements of the *E. coli* culture. This difference could be due to differing psychrometric effects between the *in situ* measurements made with the μTM and *ex situ* measurements performed with the WP4C. The higher water activity

DOI: 10.1021/acs.analchem.9b02647
Anal. Chem. 2020, 92, 716−723

(potential) relative to the WP4C measured by the μTM in the *E. coli* culture could be due to the μTM being at a lower temperature than the culture. This temperature difference could be a result of the influence of room temperature on the μTM due to poor insulation or thermal conduction through the electrical leads. However, this conjecture seems unlikely. If this higher water activity (potential) measurement relative to the WP4C was due to the μTM being at a lower temperature, we would expect that other *in situ* measurements performed on a cold block of cheese would be lower than the WP4C measurement. We are, therefore, unsure why these measurements differ to this extent.

CONCLUSION

In summary, we have presented methods which allow a MEMS tensiometer to perform water activity measurements on a wide variety of samples. Exploiting capillarity and liquid water under tension, the μTM measures water activity as a difference in pressure between a volume of pure water within the tensiometer and the ambient pressure. Due to its increased range ($1 < a_w < \sim 0.93$) compared to a conventional tensiometer ($1 < a_w < \sim 0.999$), we demonstrate that the μTM can be used to make water activity measurements across a variety of contexts previously inaccessible to tensiometry. Its small size and microfabricated design enable the μTM to be a versatile sensor for making *in situ* as well as *ex situ* measurements of water activity (potential). We demonstrate that the μTM can make accurate *in situ* measurements on samples relevant to food (e.g., cheeses, breads, juices) and biotechology (e.g., cell cultures) industries. To our knowledge, existing technologies for the measurement of water activity have not allowed for this convenient mode of operation in which the sensor serves as a dippable probe that can be directly submerged in the medium of interest.

The packaging strategies we developed allow for the sensor to be successful in (1) allowing accurate, stable, and reproducible measurements of water potential in a variety of applications, (2) providing chemical, mechanical, and electrical protection for our MEMS chip, and 3) promoting equilibrium between the μTM and sample.

In our work with these packaging and measurement methods, we have identified several areas that would benefit from further development such as (1) in *ex situ* measurements, actively controlling μTM temperature as well as sample temperature to better manage psychrometric effects, (2) in *in situ* measurements, improving temporary (or implementing permanent) sealing of ePTFE caps to packaged μTM to avoid leakage which can occur and ensuring the packaging material can exclude ionic solutes (e.g., NaCl), (3) increasing the diameter of the copper used in the *ex situ* measurement system to allow for better thermal contact between top and base, and (4) refining basic packaging methods for the μTM to provide more uniform results.

ASSOCIATED CONTENT

Supporting Information

The Supporting Information is available free of charge at https://pubs.acs.org/doi/10.1021/acs.analchem.9b02647.

Additional discussion of the relevance of water activity and relationships between thermodynamic state variables associated with water activity; full details on fabrication, packaging, and calibration procedures; additional details on the *ex situ* measurement system; procedure for extracting equilibrium values from data sets like Figure 3; discussions of sources of uncertainty and uncertainty analysis; comments on the impact of the psychrometric effect; and comparison of the transients of microtensiometers with and without veins. (PDF)

AUTHOR INFORMATION

Corresponding Author

*E-mail: ads10@cornell.edu. Phone: (607) 255-4276.

ORCID

Winston L. Black, II: 0000-0001-7811-4153

Present Address

[‖]M. Santiago: FloraPulse Co., Davis, California, 95618, United States.

Notes

The authors declare the following competing financial interest(s): Co-authors M.S. and A.D.S. have a financial interest in FloraPulse Co., a company that holds a license to commercialize the microtensiometer used in this study.

ACKNOWLEDGMENTS

The authors would like to acknowledge the technical assistance of Glenn Swan for his machining work and Morgan Ludwicki for her help with the cell culture experiments. We thank Pierre Lidon for his help with uncertainty analysis and for providing Python scripts. The authors are also indebted to the authors and contributors to the programing language, Python,[19] and the following scientific computing packages: Matplotlib,[20] SciPy,[21] and NumPy.[22] We thank METER group (formerly Decagon Devices) for their contribution of the WP4C dew point hygrometer under a Grant A. Harris Fellowship awarded to M.S. W.B. and M.S. acknowledge the support of graduate research fellowships from the NSF (DGE-1650441) as well as Sloan Fellowships from the Alfred P. Sloan Foundation. This project was supported by AFOSR (FA9550-15-1-0052), USDA (2015-67021-22844), and NSF (1721708) and was performed, in part, at the Cornell NanoScale Science and Technology Facility, a member of the National Nanotechnology Infrastructure Network, which is supported by the NSF (ECCS-1542081).

REFERENCES

(1) Farahani, H.; Wagiran, R.; Hamidon, M. N. *Sensors* **2014**, *14*, 7881−7939.
(2) Sweeney, T. E.; Beuchat, C. a. *Am. J. Physiol.* **1993**, *264*, R469−R480.
(3) Grattoni, A.; Canavese, G.; Montevecchi, F. M.; Ferrari, M. *Anal. Chem.* **2008**, *80* (7), 2617−2622.
(4) DIXON, M. A.; TYREE, M. T. *Plant, Cell Environ.* **1984**, *7* (9), 693−697.
(5) Visscher, G. J. W. *Meas. Sci. Technol.* **1995**, *6*, 1451−1461.
(6) Gee, G.; Campbell, M.; Campbell, G.; Campbell, J. *Soil Sci. Soc. Am. J.* **1992**, *56* (4), 1068−1070.
(7) Blyth, J.; Millington, R. B.; Mayes, A. G.; Frears, E. R.; Lowe, C. R. *Anal. Chem.* **1996**, *68* (7), 1089−1094.
(8) Kokoric, V.; Theisen, J.; Wilk, A.; Penisson, C.; Bernard, G.; Mizaikoff, B.; Gabriel, J. C. P. *Anal. Chem.* **2018**, *90* (7), 4445−4451.
(9) Pagay, V.; Santiago, M.; Sessoms, D. a; Huber, E. J.; Vincent, O.; Pharkya, A.; Corso, T. N.; Lakso, A. N.; Stroock, A. D. *Lab Chip* **2014**, *14* (15), 2806−2817.
(10) Slatyer, R. O.; Taylor, S. A. *Nature* **1960**, *187*, 922−924.

DOI: 10.1021/acs.analchem.9b02647
Anal. Chem. 2020, 92, 716−723

(11) Santiago, M. *Transport and Thermodynamics of Water in the Biosphere*; Ph.D.Thesis, Cornell University, 2016.
(12) Zhu, S. *In-Plant Applications of a Micro-Tensiometer Water Stress Sensor*; M.S. Thesis, Cornell University, 2017.
(13) Taylor, J. R. *An Introduction to Error Analysis: The Study of Uncertainties in Physical Measurements*, 2nd ed.; University Science Books, 1997.
(14) Seiler, F. A. *Risk Anal.* **1987**, 7 (4), 509−518.
(15) Devore, J. L. *Probability and Statistics for Engineering and the Sciences*, 7th ed.; Brooks/Cole, 2009.
(16) *WP4C Dewpoint PotentiaMeter Operator's Manual*; Decagon Devices, Inc., 2013; p 57.
(17) *Water Potential Products*, EllTech Group Wescor. http://water.wescor.com (accessed December 2019).
(18) *PSY1 Psychrometer*, ICT International. http://au.ictinternational.com/products/psy1/psy1-stem-psychrometer/ (accessed December 2019).
(19) *Python Language Reference*, version 3.6. Python Software Foundation. http://www.python.org (accessed December 2019).
(20) Hunter, J. D. *Comput. Sci. Eng.* **2007**, *9* (3), 90−95.
(21) Oliphant, T. E. *Comput. Sci. Eng.* **2007**, *9* (3), 10−20.
(22) Oliphant, T. E. *Guide to NumPy*; Trelgol Publishing, 2006.

DOI: 10.1021/acs.analchem.9b02647
Anal. Chem. 2020, 92, 716−723